Chemical Engineering Journal 534 (2026) 175168

Contents lists available at ScienceDirect

Chemical Engineering Journal

journal homepage: www.elsevier.com/locate/cej

Continuous dehydrogenation of perhydro benzyltoluene in a three-phase stirred tank slurry reactor

Elisabeth Herzinger [a], Jona Berger [a], Moritz Wolf [a,b,*]

[a] Karlsruhe Institute of Technology (KIT), Institute of Catalysis Research and Technology, Hermann-von-Helmholtz-Platz 1, 76344, Eggenstein-Leopoldshafen, Germany
[b] Karlsruhe Institute of Technology (KIT), Engler-Bunte-Institut, Engler-Bunte-Ring 1, 76131, Karlsruhe, Germany

ARTICLE INFO

Keywords:
Benzyltoluene
Dehydrogenation
Hydrogenation
Liquid organic hydrogen carrier
Slurry reactor
Stirred tank reactor

ABSTRACT

Liquid organic hydrogen carriers (LOHCs) offer a promising solution for the safe and scalable storage and transportation of hydrogen. While efficient hydrogenation is less of a challenge, technical dehydrogenation poses multifold hurdles due to its endothermic nature, slow kinetics, and highly dynamic three-phase conditions. This study presents use of a continuous three-phase stirred tank slurry reactor for the dehydrogenation of the LOHC perhydro benzyltoluene as an alternative to conventional fixed-bed reactor concepts. The slurry reactor was evaluated systematically by variation of stirrer speed, feed rate, and operation temperature to identify operating regimes enabling stable and controlled hydrogen release under continuous three-phase conditions. Long-term operation under technically relevant temperature and pressure levels demonstrated stable operation with efficient phase separation, sustained catalyst activity, and minimal LOHC degradation. At 310 °C, a stable Pt-based hydrogen productivity of 2.7 $g_{H2}\ g_{Pt}^{-1}\ min^{-1}$ and a degree of dehydrogenation of approx. 40% were obtained, which indicates efficient catalyst utilisation when compared to other reported reactor concepts. Restart experiments showed that mechanical agitation effectively restores performance after shutdown. However, repeated rapid on-off cycles led to temporary deviations from steady-state. In addition, continuous hydrogenation was demonstrated using a catalyst basket configuration, achieving a degree of hydrogenation of 99.9% and confirming the general suitability of the continuous stirred tank reactor (CSTR) configuration for reversible LOHC operation. Overall, the study positions the three-phase slurry CSTR as a complementary reactor concept emphasising catalyst efficiency, thermal homogeneity, and operational stability under continuous operation.

1. Introduction

The transition of the energy sector from fossil fuels to sustainable alternatives is one of the most pressing challenges of our time and essential to mitigate climate change and its consequences.[1,2] Hydrogen is a highly versatile chemical energy carrier that can complement electricity in a low-carbon economy offering solutions for heat, transport, power system balancing, long-term energy storage, as well as a feedstock in chemical industry. Unlike electricity, real-time matching or co-location of supply and demand is not a prerequisite, which allows for a greater flexibility in decarbonisation via a global energy transition.[3] However, the implementation of a functional hydrogen economy depends not only on efficient production and end-use technologies, but also on the development of robust storage and distribution solutions. This is of particular significance because the low volumetric energy density of hydrogen, alongside high diffusivity and flammability, results in challenges with respect to storage, transportation, and handling.[4]

Liquid Organic Hydrogen Carriers (LOHCs) are considered an effective solution addressing the challenging handling of molecular hydrogen as they enable safe, efficient, and scalable storage and transportation while using existing liquid fuel infrastructure. LOHCs chemically bind hydrogen, which retains the beneficial properties of the carrier molecules, such as being liquid under ambient conditions, addressing many of the safety, storage, and logistical issues associated with hydrogen gas. Their reversibility and economic advantages make them a promising technology for advancing the hydrogen economy.[5–8]

In recent years, a variety of reactor concepts have been developed to overcome the challenges of LOHC dehydrogenation, with each design aiming at improving hydrogen yield, energy efficiency, scalability, or

* Corresponding author at: Karlsruhe Institute of Technology (KIT), Institute of Catalysis Research and Technology, Hermann-von-Helmholtz-Platz 1, 76344, Eggenstein-Leopoldshafen, Germany.
E-mail address: moritz.wolf@kit.edu (M. Wolf).

https://doi.org/10.1016/j.cej.2026.175168
Received 10 December 2025; Received in revised form 4 March 2026; Accepted 11 March 2026
Available online 12 March 2026

integration potential. The choice of reactor type depends on both technical performance and suitability for specific applications, such as stationary large-scale systems or mobile, decentralised use. To date, fixed-bed reactors represent state-of-the-art technology. In these systems, the catalyst is typically loaded as a randomly packed bed of shaped catalyst bodies.[9–13] Their appeal lies in their robustness, simplicity, scalability, and they provide a high hydrogen output during continuous operation. However, the strongly endothermic nature of the dehydrogenation provides several challenges for fixed-bed reactors. These include hindered heat transfer through the multiphase (gas-liquid-solid) packed bed with an increased risk of catalyst and LOHC degradation at the reactor wall, particularly under dynamic load changes. Further, dewetting of the catalyst due to the release of large volumes of hydrogen limits the productivity of a large fraction of the catalyst while accelerating side product formation and even coking.[9] These limitations have motivated the investigation of alternative reactor concepts at laboratory scale. For example, multi-stage membrane reactors facilitate hydrogen removal from the reactor, which limits dewetting and shifts the equilibrium conversion to the products while simultaneously enabling hydrogen purification.[14–16] Reactive distillation provides an improved heat integration and also shifts the thermodynamic equilibrium toward dehydrogenation by continuously removing hydrogen and enriching hydrogen-rich LOHC molecules in the reaction zone.[17,18] Beyond separation-driven designs, intensified mixing strategies have also been proposed. The swirling flow reactor concept enhances radial mixing and heat transfer through a helical motion of the fluid,[19] while the triple-loop rotating cage concept promotes intense cyclic flow.[20] This leads to improved gas-liquid-solid contact, efficient utilisation of catalysts, and reduced mass transfer limitations.[19,20] Meanwhile, microchannel and structured reactors deliver exceptionally high heat and mass transfer rates, respectively, thereby enhancing the efficiency of the hydrogen release.[14–16,21,22] In this context, catalytic finned-tube reactors with washcoated tube surfaces have emerged as a promising concept employing structured reactors for LOHC dehydrogenation, which combines a large heat transfer area with near plug-flow behaviour and enables a fast dynamic response and high volumetric power densities.[23]

Innovative reactor design approaches often target individual bottlenecks. However, reactor design is always a trade-off between thermal control, scalability, integration complexity, material costs, and throughput. Amidst these considerations, stirred three-phase slurry reactors (Fig. 1) stand out as a particularly promising. Free suspension of the fine catalyst powder in the liquid phase intensifies gas-liquid and liquid-solid interfaces while minimising pressure drop. At the same time, the release of hydrogen in the slurry supresses catalyst dewetting and may enable stable long-term performance even under dynamic loads. The small particle size minimises heat and mass transport resistances, while mechanical stirring promotes uniform mixing and efficient heat input, thereby supporting isothermal operation. In line with this, Prieto et al.[24] used detailed three-phase simulations to demonstrate that slurry reactors can operate close to isothermal conditions during strongly endothermic dehydrogenation of dibenzyltoluene and indole-based LOHCs, with external transport resistances remaining small compared to intrinsic kinetics. Slurry reactors are often implemented as continuous stirred tank reactors (CSTRs) and ensure ideal mixing of the phases and a stable suspension of the catalyst while facilitating internal phase separation as well as online catalyst discharge and replacement. Their comparatively simple construction facilitates start-up and adjustments of operation conditions, as well as prolonged use.[25,26] Consequently, the CSTR configuration is a well-established design for investigating multiphase reaction kinetics under controlled and reproducible conditions. Hence, slurry systems are particularly attractive for reactor-scale kinetic evaluation and the technical dehydrogenation of LOHC.

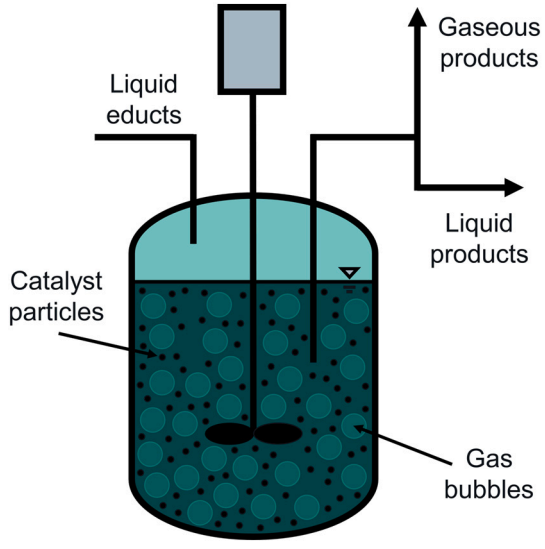

Fig. 1. Schematic of the three-phase slurry reactor concept with liquid feed, suspended catalyst particles, and a joint gas-liquid outlet with subsequent separation stage.

While fixed-bed and tubular reactor concepts are mostly used in literature on LOHC dehydrogenation, continuous three-phase stirred tank slurry operation under technically relevant conditions has not been systematically investigated. The present work therefore evaluates catalyst utilisation, operational stability, restart behaviour, and reactor-scale performance of a CSTR configuration for perhydro benzyltoluene (H12-BT) dehydrogenation and provides a structured comparison to representative fixed-bed and intensified reactor concepts. The performance of the reactor was systematically assessed by varying key operation parameters, such as stirrer speed, reactant feed rate, and temperature to optimise hydrogen release. Long-term experiments were conducted under technically relevant conditions to assess stability of operation as well as catalyst and LOHC durability. In addition, start-up and shutdown procedures were investigated to evaluate operational robustness and dynamicity. The study also includes a demonstration of the hydrogenation capability of the system and evaluates the reactor design with respect to process efficiency and practical applicability, particularly in the context of stationary LOHC-based energy storage applications.

2. Experimental

2.1. Materials

All experiments were carried out using commercially available catalysts by Clariant Produkte GmbH, which were supplied by Hydrogenious LOHC Technologies (Germany). EleMax D catalyst (PtS/Al_2O_3) was used for dehydrogenation. This selectively poisoned catalyst is provided as an egg-shell catalyst in the form of spherical bodies measuring 2–4 mm. For use in the slurry reactor, the catalyst was ground and sieved into particle size fractions >63 µm and <125 µm to prevent blockage of the frit or downstream filters by fines while maintaining good suspendability and minimising limitation due to internal diffusion. EleMax H catalyst (1.8 mm spheres of $PtPd/Al_2O_3$) was applied for hydrogenation without further treatment. Catalyst particle size was selected according to the specific objective of each experiment (slurry suspension performance for dehydrogenation versus operability/handling robustness for hydrogenation) and was not intended for direct comparison of intrinsic reaction rates between both reaction directions. The metal loading of the used catalysts was characterised via inductively coupled plasma atomic emission spectrometry. A detailed description of the method and the subsequent results can be found in the Supporting Information (SI, Table S.1). H12-BT was purchased from Hydrogenious LOHC Technologies (Germany) and contained minor impurities of

benzyltoluene (H0-BT) and partially hydrogenated benzyltoluene (H6-BT), resulting in a degree of hydrogenation (DoH) of 99.7% (Fig. S.1). H0-BT was purchased from KRAHN Chemie Deutschland (Germany) with a DoH of 0% (Fig. S.2). Argon (ALPHAGAZ 2, quality 6.0, >99.9999 mol%) and hydrogen (ALPHAGAZ 1, quality 5.0, > 99.999 mol%) were supplied by Air Liquide.

2.2. Reactor set-up

Catalytic hydrogenation and dehydrogenation of (perhydro) benzyltoluene was conducted in a CSTR (Parr Instruments, Fig. 2), consisting of a 450 ml pressure vessel equipped with a mechanical stirrer and electrical heating. The internal components include a 35 mm pitched-blade stirrer, a cooling coil, a thermocouple and a pressure gauge.

The continuous feed of LOHC is provided by an HPLC pump. Inert gas (Ar) or hydrogen (H_2) can be introduced above the liquid level of the reactor via mass flow controllers. The products leave the reactor via a customised two-phase outlet consisting of a dip tube with frit for the liquid and a side-mounted frit for the gas phase (Fig. S.3), which ensures a working reaction volume of approx. 270 ml without pressure build-up by entraining liquid with the exiting gas flow.

Gas-liquid separation is realised in a counterflow condenser, cooled to 1 °C using a circulating chiller, and a downstream buffer tank with liquid and gas outlets. The system pressure is regulated via a back-pressure regulator (BPR). A thermal conductivity detector (TCD) enables in-line gas analysis via quantification of hydrogen in the sweep gas argon, which is either directed through the gas phase of the reactor and subsequent separation stage or via a bypass to the TCD. The LOHC level in the buffer tank is controlled by two level sensors and a pneumatic on/off valve. Liquid LOHC is either discharged to a product container or sampled at intervals using an autosampler (Autosam 360, HiTec Zang).

2.3. Experimental procedure

For each dehydrogenation experiment, 250 ml of H12-BT were loaded into the reactor. The system was flooded with additional H12-BT at a feed rate of 2.0 ml min^{-1} while flowing 200 ml min^{-1} of argon as sweep gas until the pneumatic on-off valve opened and closed

Table 1
Standard operation parameters for the dehydrogenation at atmospheric pressure including parameter variations in parentheses, as well as operation parameters for hydrogenation and long-term dehydrogenation under technically relevant conditions.

Parameter	Dehydrogenation (variations)	Long-term dehydrogenation	Hydrogenation (variations)
Pressure / bar_a	1.0	4.3	32.1
Temperature / °C	250 (250…210)	310	250
Stirrer speed / rpm	1000 (250…1750)	1000	1000
Impeller	Pitch-blade stirrer	Pitch-blade stirrer	Gassing impeller
Catalyst	EleMax D	EleMax D	EleMax H
Catalyst amount / g	7.16	7.16	26.90
Catalyst type	Ground powder (63–125 µm)	Ground powder (63–125 µm)	Spheres (1.8 mm)
Catalyst basket	No	No	Yes
Reaction volume / ml	~270	~270	~155
Liquid feed / ml min^{-1}	2.0 (2.0, 1.0, 0.5)	2.0	2.0 (1.0, 0.5)
Ar flow / ml_N min^{-1}	200	–	–
H_2 flow / ml_N min^{-1}	–	100	1000

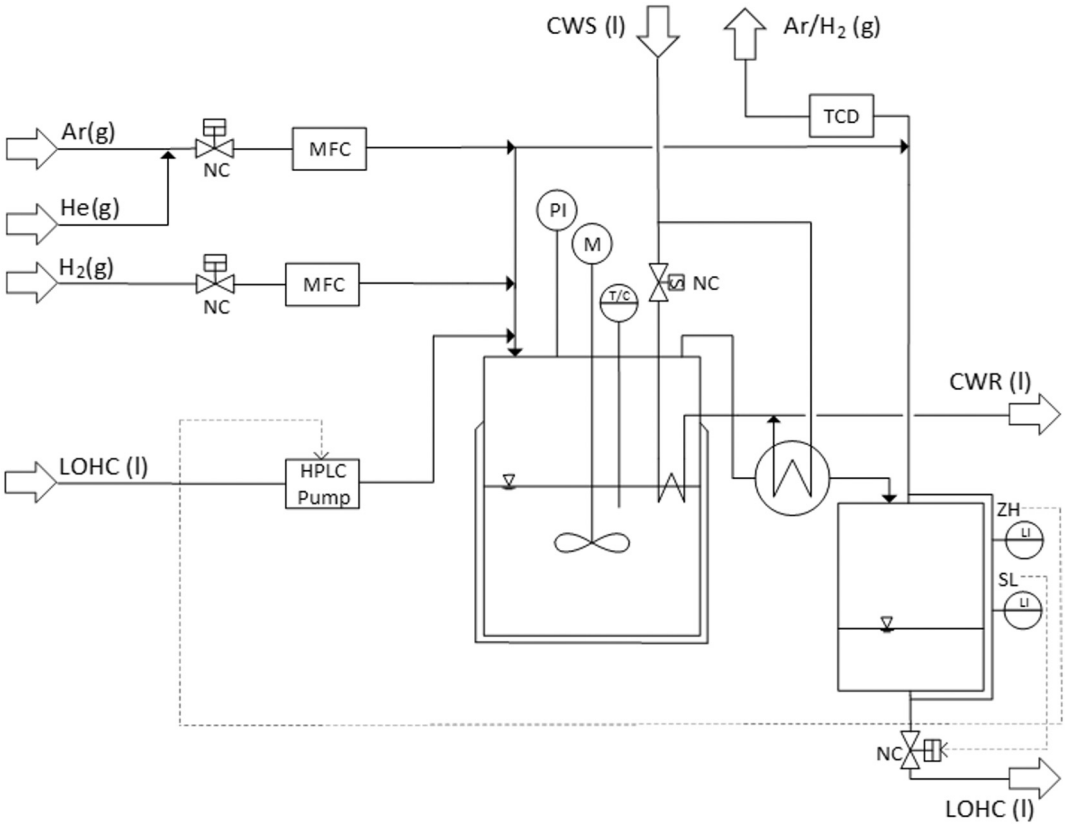

Fig. 2. Flow scheme of continuous stirred tank reactor with a downstream buffer tank for liquid-gas separation.

periodically. After flooding, the reactor was opened and a certain amount of the dehydrogenation catalyst EleMax D was added as ground powder (Table 1). EleMax D was selected to enable direct comparison with literature benchmarks on H12-BT dehydrogenation by employing the same commercially available catalyst. The reactor was purged again with 200 ml min^{-1} of argon until a stable signal was obtained for the thermal conductivity detector. Heating was initiated alongside the gas flow and stirring. A set of standard operating parameters was selected for all parameter variations during dehydrogenation experiments (Table 1). Ar was applied as sweep gas during dehydrogenation to stabilise the gas flow to the online analytics, which is particularly important when only small amounts of H_2 are released. As demonstrated in the results section, the additional Ar flow stabilises the signal without significantly altering the qualitative release rates during dehydrogenation. Once the temperature in the reactor reached 230 °C, the H12-BT feed and automated sampling were started simultaneously. After reaching the set temperature, the reactor was operated under steady conditions for at least five hours and the individual process parameters (stirrer speed, H12-BT feed rate, or temperature) were varied separately for minimum four hours each.

A modified procedure (Table 1) was applied for a long-term experiment conducted under elevated pressure resembling technically relevant conditions. In this case, hydrogen was used instead of argon for the initial flooding, with the pressure being released before the reactor was opened to add the catalyst. Prior to heating, the target system pressure was adjusted with hydrogen using the BPR. A small H_2 sweep flow was used during the experiment to ensure stable pressure regulation by the BPR, gas-throughput stabilisation and constant pressure, especially during small net H_2 release. Argon was only introduced for the gas analysis via TCD using the bypass.

To test the re-start behaviour of the system, an experiment with multiple start-up und shutdown periods was performed. The reactor was operated under standard conditions (second column in Table 1) and was kept running for eight mean residence times before the first shutdown. Subsequently, the heating was switched off, the gas and liquid feeds were stopped and the reactor was actively cooled. Once room temperature was reached, stirring was stopped and the reactor was left in this state for 24 h. The reaction was then restarted using the standard start-up procedure. This procedure was repeated eight times with dedicated downtimes between 12 and 100 h. At two distinct periods of time, the argon flow was bypassed with no flow through the reactor to assess the potential influence argon flushing through the gas phase in the reactor.

For hydrogenation, 250 ml of H0-BT were loaded into the reactor, the reactor was closed, and the pressure was increased to 32.1 bar_a with a hydrogen flow of 1000 ml min^{-1} and a reactant feed rate of 2.0 ml min^{-1}. As the system reached a stable operation and the automated product valve at the liquid outlet opened at regular intervals, the pressure was released and the reactor was opened to insert the hydrogenation catalyst EleMax H employing a catalyst basket (Fig. S.4), which was completely filled with the spherical (1.8 mm) catalyst bodies. EleMax H was selected for hydrogenation because sulfur-containing dehydrogenation catalysts (e.g. EleMax D) may release H_2S at high H_2 partial pressures, which can compromise the safety of long-term operation and can damage reactor components. A gassing impeller was used to ensure gas entry into the liquid phase and maximised biphasic flow through the catalyst basket. The reactor was closed and the pressure was increased under stirring and hydrogen flow. At operation pressure, heating was initiated and the reactant feed was activated when the reactor temperature reached 210 °C. The reactor was operated under steady conditions for six mean residence times and afterwards the reactant feed rate was varied (Table 1).

2.4. Mixing performance and suspension behaviour

Variation of the stirrer speed can be described by the dimensionless Reynolds number *Re*. For a stirred tank, *Re* is calculated using the density of the reaction mixture ρ, the impeller rotation speed n in s^{-1}, the impeller diameter D (35 mm), and the dynamic viscosity η according to Eq. (1).[27,28]

$$\mathrm{Re} = \frac{\rho\, n\, D^2}{\eta} \tag{1}$$

The effect of solids is not taken into account for the Reynolds number for stirred suspensions. According to Zwietering's correlation (Eq. (2) and SI), complete suspension is achieved when the impeller speed exceeds the impeller speed for just-suspended particles n_{js}. This correlation accounts for the influence of fluid properties, particle characteristics, and impeller geometry on the onset of complete suspension using a dimensionless number S (Eq. (S.21)), kinematic viscosity ν, gravitational acceleration constant g (9.81 m s^{-2})[29], density of solid ρ_s and liquid ρ_l phases, mass ratio of suspended solids to liquid x, mass-mean particle diameter d_p, and impeller diameter D (35 mm).[28,30]

$$n_{js} = S\nu^{0.1}\left[\frac{g(\rho_s - \rho_l)}{\rho_l}\right]^{0.45} x^{0.13} d_p{}^{0.2} D^{-0.85} \tag{2}$$

2.5. Key performance indicators

The flow of hydrogen out of the reactor was quantified using the pre-calibrated in-line TCD. The hydrogen concentration in argon x_{H2} is converted into a volumetric hydrogen flow V_{H2} based on the set volume flow of argon V_{Ar} (Eq. (3)). In the case of hydrogen overflow in the reactor, the measured volumetric flow of hydrogen is subtracted from the set flow of the MFC during hydrogenation to quantify hydrogen consumption.

$$\dot{V}_{H_2} = \frac{x_{H_2} \bullet \dot{V}_{Ar}}{1 - x_{H_2}} \tag{3}$$

A precious metal based catalyst productivity (Prod.) can be determined according to Eq. (4) using the volumetric hydrogen flow, the catalyst mass $m_{cat.}$, the catalyst loading w, and the density of hydrogen ρ_{H2} (0.0898 kg m^{-3} at 273.15 K and 100 kPa)[31]. This descriptor for the catalyst activity relates the mass of released hydrogen m_{H2} per unit of time Δt to the mass of catalytically active platinum m_{Pt} during dehydrogenation experiments, while the total loading of platinum and palladium was accounted for during hydrogenation.

$$\mathrm{Prod.} = \frac{\dot{V}_{H_2} \bullet \rho_{H_2}}{w \bullet m_{cat.}} = \frac{m_{H_2}}{m_{Pt} \bullet \Delta t} \tag{4}$$

The reactor stability was assed using the relative change in productivity related to dimensionless time ΔProd.(θ) as a steady-state indicator, where θ denotes the dimensionless time defined as the ratio of the time on stream t to the mean residence time τ (Eq. (S.2)). To compare the degree of stabilisation between operating conditions, three stability levels were defined (Table 2), while steady-state was generally defined as a deviation <3%.

The space-time yield (STY) was determined as a measure for the volumetric productivity by relating the molar flow of products $\dot{n}$ to the volume V.[32] The STY was calculated according to Eq. (5) using the volumetric hydrogen flow rate V_{H2}, the reaction Volume V_R, and conversion of the volumetric flow into a molar flow using the molar gas volume under standard conditions V_m (22.4 l mol^{-1})[33].

Table 2
Classification of steady-state criteria according to the relative change in productivity per dimensionless time.

Steady-state criterion	ΔProd.(θ) / %
Loose	<3
Moderate	<2
Strict	<1

$$\mathrm{STY} = \frac{\dot{n}}{V} = \frac{\dot{V}_{H_2}}{V_m\, V_R} \tag{5}$$

The degree of dehydrogenation (DoD) is defined as the molar amount of released hydrogen $n_{H2,released}$ and the maximum capacity for reversibly bound hydrogen in the LOHC $n_{H2,rev.\max}$. In practice, the released hydrogen is obtained by subtracting the residual amount of reversibly bound hydrogen at the reactor outlet $n_{H2,rev.out}$ from $n_{H2,rev.max}$ (Eq. (6)). Accordingly, the DoD can be calculated using Eq. (7).

$$n_{H_2,released} = n_{H_2,rev.max} - n_{H_2,rev.out} \tag{6}$$

$$\mathrm{DoD} = \frac{n_{H_2,released}}{n_{H_2,rev.max}} \bullet 100\% = \left(1 - \frac{n_{H_2,rev.out}}{n_{H_2,rev.max}}\right) \bullet 100\% \tag{7}$$

Using a molar material balance for the reactor, the DoD can be derived from the quantified flow of released hydrogen according to the TCD ($\mathrm{DoD_{TCD}}$) assuming ideal backmixing and a constant liquid reaction volume. The detailed mathematical derivation is provided in the SI (Eqs. (S.5)-(S.13)). In short, a virtual concentration of hydrogenated BT equivalents $c_{Hx\text{-}BT}$ at the reactor outlet is derived over time t from the released hydrogen and related to the inlet concentration of H12-BT $c_{H12\text{-}BT}$ as expressed in Eq. (8).

$$\mathrm{DoD_{TCD}}(t) = \left(1 - \frac{c_{Hx-\mathrm{BT}}(t)}{c_{H12-BT}}\right) \bullet 100\% \tag{8}$$

As the DoH is the complementary measure of the DoD, it can be determined from the molar amount of reacted moles of hydrogen $n_{H2,consumed}$ and $n_{H2,rev.\max}$ (Eq. (9)).

$$\mathrm{DoH} = \frac{n_{H_2,consumed}}{n_{H_2,rev.max}} \bullet 100\% \tag{9}$$

By linking the time-resolved signal from gas analysis with the reactor content via the CSTR balance (Eqs. (S.14)-(S.20)), the net hydrogen uptake can be used to determine the molar amount of H0-BT remaining in the vessel $n_{H0\text{-}BT}$. The $\mathrm{DoH_{TCD}}$ can be obtained by normalisation using the value in the feed, $n_{H0BT,0}$, as defined in Eq. (10).

$$\mathrm{DoH_{TCD}}(t) = \left(1 - \frac{n_{H0-BT}(t)}{n_{H0-BT,0}}\right) \bullet 100\% \tag{10}$$

The conversion X is defined as the relative decrease in the molar amount n of a component i and can be calculated using the molar amount in the feed $n_{i,0}$ and the molar amount at the reactor outlet n_i using Eq. (11). If the target of the reaction is hydrogen release (dehydrogenation), the conversion is based on the difference between the molar amount of hydrogen reversibly bound to the LOHC in the liquid feed $n_{H2,rev.in}$ and the liquid at the reactor outlet $n_{H2,rev.out}$. For a fully hydrogenated liquid feed ($n_{H2,rev.in} \approx n_{H2,rev.\max}$), the conversion of dehydrogenation X_{DoD} can be approximated by the DoD using Eq. (12). The conversion of hydrogenation X_{DoH} can be expressed on the basis of the maximum hydrogen capacity of the H0-BT $n_{H2,rev.max}$ and the consumed hydrogen $n_{H2,consumed}$ obtained from the hydrogen inflow $n_{H2,in}$ and the outflow $n_{H2,out}$, which can as well be approximated using the DoH (Eq. (13)).

$$X = \frac{n_{i,0} - n_i}{n_{i,0}} \tag{11}$$

$$X_{\mathrm{DoD}} = \frac{n_{H_2,rev.in} - n_{H_2,rev.out}}{n_{H_2,rev.in}} \approx \frac{\mathrm{DoD}}{100\%} \tag{12}$$

$$X_{\mathrm{DoH}} = \frac{n_{H_2,in} - n_{H_2,out}}{n_{H_2,rev.max}} = \frac{n_{H_2,consumed}}{n_{H_2,rev.max}} \approx \frac{\mathrm{DoH}}{100\%} \tag{13}$$

2.6. Analysis of liquid samples

Liquid samples from the auto sampler were analysed using gas chromatography (GC 8890, Agilent Technologies, Inc.) equipped with a DB-17 ms column (length: 30 m; inner diameter: 250 µm) and flame ionisation detection (FID). Approx. 100 µl of the liquid sample were diluted in 0.9 ml of isopropanol. An aliquot (1 µl) of this solution was then injected in the GC and separated using a predefined temperature programme (Table S.2). In addition, a liquid sample from the reactor was analysed at the end of the long-term experiment and labelled 'Reactor sample' (Table S.11).

GC-FID analysis allows for distinct separation of the individual BT species, namely H12-BT, H6-BT, H0-BT, the major by-product methylfluorene (Fl),[34] as well as other high-boiling compounds (HB), formed during the reaction. Raw chromatographic signals were processed in Python, with peak areas serving as the basis for quantification. Mole fractions of the individual BT species $x_{Hx\text{-}BT}$ were determined and subsequently used to calculate the $\mathrm{DoH_{GC}}$ according to Eq. (14). The $\mathrm{DoD_{GC}}$ can be calculated from the $\mathrm{DoH_{GC}}$ using Eq. (15).

$$\mathrm{DoH_{GC}} = \left[\frac{12}{12} \bullet x_{H12-BT} + \frac{6}{12} \bullet x_{H6-BT} + \frac{0}{12} \bullet (x_{H0-BT} + x_{Fl} + x_{HB})\right] \bullet 100\% \tag{14}$$

$$\mathrm{DoD_{GC}} = 100\% - \mathrm{DoH_{GC}} \tag{15}$$

2.7. Kinetic analysis of dehydrogenation

For comparative purposes, the effective reaction rate is normalised to the mass of the active catalytic component $m_{act.comp.}$ yielding $r_{i,eff}$ as defined in Eq. (16).[25] This quantity depends on the reactant concentration c_i, the effective reaction order n_{eff} and the temperature dependant effective rate constant k_{eff}.

$$r_{i,eff} = \frac{1}{m_{act.comp.}} \frac{dn_i}{dt} = -k_{eff}(T) \bullet c_i^{\,n_{eff}} \tag{16}$$

To calculate the effective formation rate of hydrogen $r_{H2,eff}$, the productivity and the molar mass of hydrogen M_{H2} (2.016 g $\mathrm{mol^{-1}}$)[31] were used alongside conversion of units as described by Eq. (17). Using the stoichiometric relationship established in Eq. (S.10), $r_{H2,eff}$ can also be expressed via the effective rate constant k_{eff}, the concentration of hydrogenated BT equivalents $c_{Hx\text{-}BT}$, and the effective reaction order n_{eff} (Eq. (17)), while the factor 6 accounts for the release of six moles of hydrogen per H12-BT for complete dehydrogenation.

$$r_{H_2,eff} = Prod. \ \frac{1}{M_{H_2}} \frac{1000\ g_{Pt}}{1\ kg_{Pt}} \frac{1\ min}{60\ s} = 6 \bullet k_{eff} \bullet c_{Hx-BT}^{\,n_{eff}} \tag{17}$$

While the productivity is obtained from TCD measurements, the concentration $c_{Hx\text{-}BT}$ is determined from GC data by combining the mole fractions $x_{H12\text{-}BT}$ and $x_{H6\text{-}BT}$ with the molar mass $M_{BT\text{-}mix}$ and density ρ_{BT_mix} of the BT mixture (Eq. (18)). The properties of Hx-BT mixtures can be approximated from pure component data under ideal mixing (Eqs. (S.22) and (S.23)).

$$c_{Hx-BT} = \left(x_{H12-BT} + \frac{1}{2} x_{H6-BT}\right) \frac{\rho_{BT-mix}}{M_{BT-mix}} \tag{18}$$

The effective rate constant k_{eff} is determined from $r_{H2,eff}$ obtained from Eq. (17) and $c_{Hx\text{-}BT}$ according to Eq. (19) assuming a reaction order of 1. This description is in accordance with the Arrhenius law, where k_0 is the pre-exponential factor corresponding to the rate constant k_{eff} at infinitely high temperatures, $E_{A,e}$ is the Arrhenius activation energy, R is the universal gas constant, and T is the absolute temperature.[32]

$$k_{eff}(T) = \frac{r_{H_2,eff}}{6 \bullet c_{Hx-BT}} = k_0 \bullet exp\left[\frac{-E_{A,e}}{RT}\right] \tag{19}$$

When using the natural logarithm of Eq. (19) according to Eq. (20), a linear relationship is obtained, while k_0 and $E_{A,e}$ can be determined in the Arrhenius plot using the slope and y-axis intercept, respectively.

$$\ln(k_{eff}) = \ln(k_0) - \frac{E_{A,e}}{R}\frac{1}{T} \quad (20)$$

3. Results and discussion

3.1. Proof-of-concept and role of the stirrer speed

Step function tracer experiments were conducted to determine the RTD of the reaction system comprising the reactor with the subsequent buffer tank system for gas-liquid separation, which is discussed in detail in the SI (Fig. S.5). The analysis with a tracer feed rate of 2.0 ml min^{-1} suggests that the reactor provides the anticipated well-mixed response, while the buffer tank and lines in the downstream section introduce a delay of 40 min. The residence time of the reactor-buffer tank system τ_{total} at this feed rate was determined to be 175 min with a mean reactor residence time $\tau_{reactor}$ of 135 min.

First dehydrogenation experiments were performed at 250 °C with a H12-BT reactant feed rate of 2.0 ml min^{-1} using a ground commercially available EleMax D Pt-based catalyst. As the reactor temperature approached 250 °C, hydrogen release was observed and the DoD increased as evidenced from the analysis of liquid samples from the system outlet. After an initial spike in productivity due to the fully hydrogenated LOHC in the reactor and liquid feed, a constant hydrogen release was observed for θ >4 (Fig. 3). The defined criterium for steady state (ΔProd.(θ) <3%) was fulfilled after approx. six mean residence times. To evaluate reproducibility of the reactor performance, three independent experiments were conducted under identical conditions (250 °C, 1000 rpm, 2 ml min^{-1}). The obtained Pt-based hydrogen productivity was 0.488, 0.500, and 0.500 $g_{H2}\ g_{Pt}^{-1}\ min^{-1}$ (Table S.3, Table S.6, Table S.9), which corresponds to a relative deviation below 2%. The space-time yield and degree of dehydrogenation exhibited a similarly high reproducibility. This confirms stable and reproducible reactor operation under steady-state conditions.

The effect of the mixing behaviour on the reactor performance was investigated by variation of the stirrer speed (Fig. 3). After the initial run-in phase at 1000 rpm, the stirrer speed was lowered to 250 rpm, after which it was increased in 250 rpm steps up to 1750 rpm (details in SI, Table S.3). Expectedly, lowering the stirrer speed from 1000 to 250 rpm caused a pronounced decrease in catalyst productivity of approx. 40% from 0.49 to 0.30 $g_{H2}\ g_{Pt}^{-1}\ min^{-1}$. This decline was accompanied by a similar decrease in the DoD_{GC} from 7.5% to 5.1%.

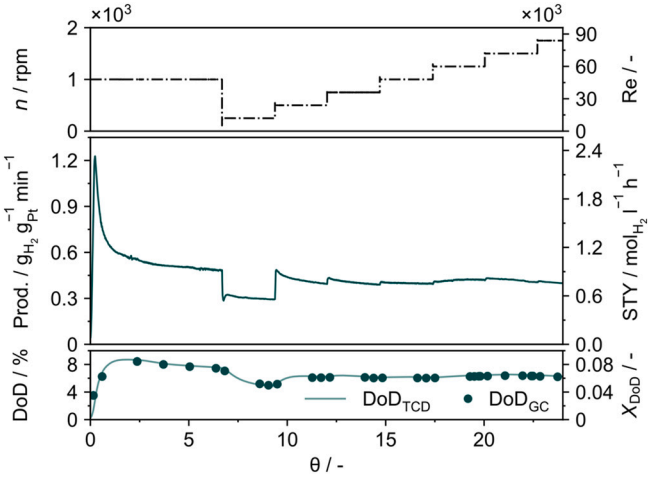

Fig. 3. Effect of the impeller speed on key performance indicators during variation of stirrer speed (250 to 1750 rpm in 250 rpm increments) and operation at 250 °C, 1 bar_a, and a H12-BT feed rate of 2.0 ml min^{-1}. The data illustrate the transition from mass-transfer-influenced operation at low impeller speeds to kinetically controlled behaviour at higher rpm, as reflected by the stabilisation of hydrogen productivity.

Partial catalyst settling due to insufficient mixing most likely reduced its accessibility for reactants. Increasing the stirrer speed to 500 rpm markedly improved productivity, reaching 0.49 $g_{H2}\ g_{Pt}^{-1}\ min^{-1}$ before gradually declining to 0.40 $g_{H2}\ g_{Pt}^{-1}\ min^{-1}$ and a DoD_{GC} of 6.1%. For a stirrer speed above 500 rpm, productivity and DoD_{GC} stabilised at 0.39–0.42 $g_{H2}\ g_{Pt}^{-1}\ min^{-1}$ and 6–6.3%, respectively, with slightly increased productivity following each setpoint adjustment. However, the relative gain decreased with each stirrer speed level. At high stirrer speeds above 1500 rpm, reactor stability decreased again, with changes exceeding the steady-state criterion. Further, the initial DoD was not fully recovered when comparing the performance at 1000 rpm before and during variation of the stirrer speed. Both observations suggest the influence of additional factors, such (temporary) catalyst unavailability due to deposition on inner parts of the reactor including the frit for solid-liquid separation when changing the stirrer speed.

To investigate the impact of stirrer speed on the stability of the suspension, the catalyst suspension was stirred in a glass beaker with dimensions similar to the reactor vessel. Visual evaluation (Fig. S.6) confirmed that complete mixing was not achieved at 250 rpm. The observations further suggest that a homogeneous suspension at room temperature is obtained above 500 rpm. However, when translated into process conditions (250 °C), this observation corresponds to a Reynolds number (Eq. (1)) that is well above the threshold for turbulent flow ($Re > 10^4$, which is reached at approx. 200 rpm, Fig. S.7). Therefore, turbulence alone is insufficient to ensure complete solid-liquid mixing, as particle suspension depends on the flow regime, particle-fluid interactions, and impeller geometry.

To provide a more accurate description for complete suspension of catalyst particles, the Zwietering correlation (Eq. (2)) was used to calculate the speed at which the catalyst is just suspended. Based on the calculations, full suspension is predicted at 645 rpm, which is consistent with the observed catalyst performance and visual inspection using a glass beaker. Here, space-time yield and conversion increase when reaching the partially suspended state, i.e. at a dimensionless stirrer speed $n\ n_{js}^{-1} = 1$ (Fig. 4). A plateau is reached for a stirrer speed >500 rpm, while additional turbulence introduced by the formed hydrogen bubbles and internal reactor components, such as cooling coil, the frit, or jackets for thermocouples, may explain deviation from Zwietering correlation at 500 rpm. At high stirrer speed in the uniform, fully suspended regime (transition from 1000 to 1250 rpm), increased space-time yields and conversions are observed suggesting optimal operation conditions. Beyond this point, in the energy-excess region, performance remains unchanged or even shows a slight decline, potentially due to enhanced catalyst deposition inside the reactor.

Overall, the results indicate that the influence of stirrer speed on catalyst performance is mostly limited to ensuring complete suspension. Above the just-suspended threshold, external transport resistances become negligible and the overall rate under given conditions is

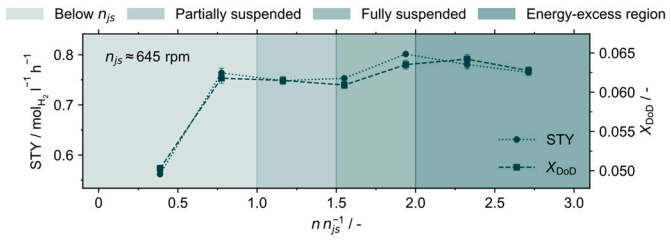

Fig. 4. Space-time yield and H12-BT conversion as a function of normalised impeller speed during variation of speed (250 to 1750 rpm in 250 rpm increments) at 250 °C, 1 bar_a, and a H12-BT feed rate of 2.0 ml min^{-1}. Data were averaged over one mean reactor residence time at the end of each setpoint. The results are compared to the characteristic suspension regimes according to the Zwietering correlation, illustrating the relationship between solid suspension quality and reactor performance. Error bars indicate the standard deviation of the data within the selected averaging window of the mean residence time.

controlled by intrinsic catalyst kinetics rather than mixing intensity. Consequently, increasing the stirrer speed further has little effect on space-time yield or conversion. Noteworthy, the operational stability declined in the over-mixed region, which is most likely linked to increased turbulence and catalyst redistribution. As high stirrer speeds also lead to unnecessary increased mechanical stress on the catalyst, a stirrer speed of 1000 rpm was selected for the following experiments.

3.2. Variation of the reactant feed rate

To investigate the influence of the reactant feed rate on mean residence time and overall reactor performance, the feed rate was systematically decreased from the standard operating conditions of 2.0 to 0.5 ml min^{-1} (Figure S.8, Table S.6). As the flow rate was decreased, the mean residence time increased leading to a longer space-time with a simultaneous increase in conversion. Normalising the performance data reveals that the increase of the conversion is more pronounced than the decrease of space-time yield (Fig. 5). While a relative gain of +51% is observed for the conversion in the first step, the space-time yield only declines by −24%. This suggests that the conversion is more sensitive to changes in the mean residence time. Therefore, even moderate changes in the feed rate significantly impact the conversion. In contrast, space-time yield is a composite performance metric reflecting both conversion and throughput, i.e. a lower throughput at lower feed rates results in decreased volumetric productivity. These opposing effects partially offset each other, resulting in a lower decline in space-time yield than in conversion. A similar trend can be observed at the second setpoint. While the relative decrease in space-time yield lies in the same magnitude (−26%), the increase in conversion was significantly smaller (+37%). This weaker response may be influenced by a lower driving force as the conversion is shifting closer to, but remains well below, equilibrium (Fig. S.9, Table S.7).

In summary, the results illustrate the inherent trade-off between achieving a high space-time yield at lower conversion levels, and ensuring efficient utilisation of the hydrogen storage capacity of H12-BT. The observed dependencies on flow rate suggest that the system under given conditions primarily operates in the kinetically controlled regime, as variations in feed rate directly affect conversion and productivity. However, at low feed rates, conversion levels off suggesting a gradual shift toward increasing influence by the thermodynamic equilibrium. From a practical perspective, a flow rate of 2.0 ml min^{-1} represents an adequate operating point, offering a balanced compromise between conversion, stable operation, and overall throughput efficiency.

3.3. Temperature variation

The temperature sensitivity of the reactor system under continuous slurry operation was studied in the range of 210 to 250 °C (Fig. S.10, Table S.9) to sustain the majority of the LOHC in the liquid phase (boiling point of isomers in the range of 264–272 °C at 1.0 bar_a).[34] Lower reaction temperatures resulted in the expected decrease in catalyst productivity and conversion, while the latter remained approx. 11–13% of the corresponding thermodynamic equilibrium conversion levels (Fig. S.9, Table S.7) throughout the experiment. Arrhenius law was applied to calculate the effective rate constant k_{eff} at each temperature level (Eq. (19)), which results in a linear correlation in the Arrhenius plot (Fig. 6a). The activation energy and pre-exponential factor (Table 3) are consistent with reported values for perhydro dibenzyltoluene dehydrogenation using commercial and non-commercial Pt-based catalysts.[35,36] Further, the temperature dependence of the effective rate constant k_{eff} (Eq. (19)) was derived for the investigated temperature range (Fig. 6b). Given the close correlation between the fits and experimental values, the Arrhenius parameters obtained from the reactor-level kinetic evaluation are validified. Overall, the results confirm that the reactor operates in a kinetically controlled regime within the investigated temperature range.

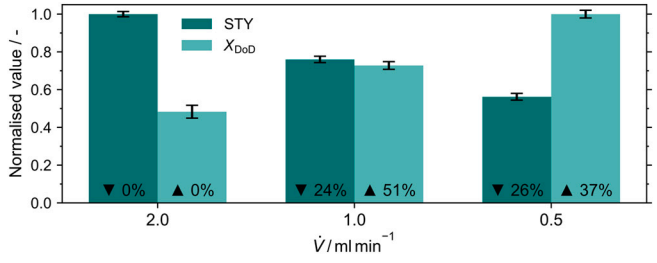

Fig. 5. Space-time-yield (STY) and conversion (X) as a function of feed rate during operation at 250 °C, 1 bar_a, and 1000 rpm. Values are normalised to the respective maximum, while ▲ and ▼ indicate the relative change in comparison to the preceding setpoint. The data illustrate the influence of residence time on reactor performance under continuous operation. Error bars indicate the standard deviation of the data within the selected averaging window of the mean residence time.

3.4. Long-term testing

Low conversion levels were targeted in the previous experiments. However, high temperature dehydrogenation is technically required to allow for reasonably high reaction rates and release of hydrogen. Therefore, the suitability of the continuous slurry reactor for hydrogen release from H12-BT was studied in a dedicated long-term experiment under steady state conditions at elevated temperature (310 °C) and pressure (4.3 bar_a) using the optimised parameters from the previous experiments. The selected pressure significantly exceeds the vapour pressure of the LOHC of 1.7 bar_a, as estimated from Eq. (S.29). The reaction was maintained under constant operating conditions for 27 mean residence times (Fig. 7, Table S.10). Following an initial induction period of approx. one mean residence time, the relative change in productivity remained within the loose steady-state criterion ($\Delta Prod.(\theta) < 3\%$) throughout the 64 h time on stream. The moderate ($\Delta Prod.(\theta) < 2\%$) and strict criterion ($\Delta Prod.(\theta) < 1\%$) are met from three and nine mean residence times onwards, respectively, indicating a high level of operational stability and a sustained catalyst activity.

When compared to the moderate operation temperatures from the previous experiments, the elevated temperature during the long-term run results in a significantly enhanced productivity and DoD of 2.7 $g_{H2}\ g_{Pt}^{-1}\ min^{-1}$ and 40.5%, respectively. The equilibrium conversion under given conditions is 84.4% emphasising the need of elevated operation temperatures for technically reasonable hydrogen release (Fig. S.9, Table S.7). Although the DoD of approx. 40% is low and does not meet one-stage reactor requirements, the operating window was deliberately selected. In LOHC dehydrogenation, increasing DoD is typically accompanied by higher required temperatures and heat fluxes due to the strongly endothermic nature of the reaction, which in turn accelerates catalyst deactivation and promotes side reactions.[37–39] Operating at intermediate DoD therefore represents a compromise between hydrogen productivity, thermal management, reactor stability, and catalyst lifetime. From a process design viewpoint, high overall hydrogen release can be achieved by employing multi-stage reactor concepts, interstage heating, or recycle loops rather than by maximising DoD in a single reactor.[15,40,41] Within such configurations, operating individual reactor stages at moderate DoD enables stable continuous operation and uniform catalyst utilisation while maintaining favourable durability. Thus, the investigated DoD range reflects a technologically relevant operating window for a single dehydrogenation stage rather than a fundamental limitation of the reactor concept. In fact, slurry reactors are ideally suited as first stage to release a large fraction of the chemically bound hydrogen, whereas the partially dehydrogenated LOHC may subsequently be fully dehydrogenated.

Due to the elevated operation temperature and increased conversion

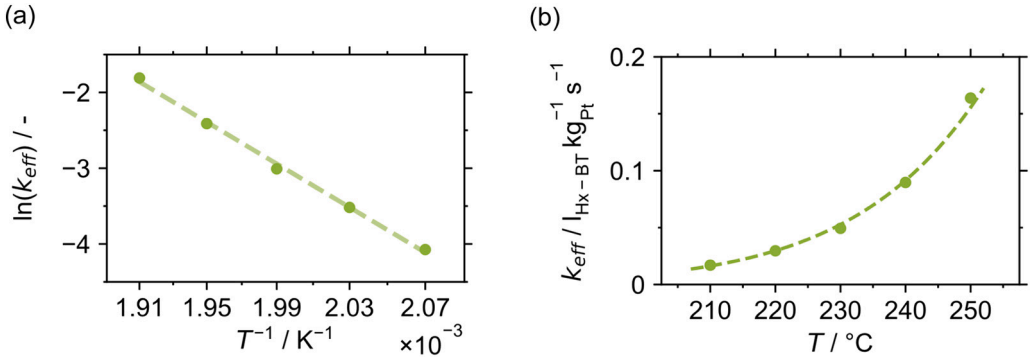

Fig. 6. (a) Arrhenius representation of the effective reactor-level rate constant with experimental values (●) and corresponding linear regression (**---**) used to determine the Arrhenius activation energy ($E_{A,e}$) and pre-exponential factor (k_0), as well as (b) temperature dependence of the effective rate constant k_{eff} (● experimental values; **—** calculated from previously determined $E_{A,e}$ and k_0) during variation of operation temperature at 1 bar_a, 1000 rpm, and a H12-BT feed rate of 2.0 ml min^{-1}. The data quantify the temperature sensitivity of the reactor system under continuous slurry operation in the studied temperature range (210–250 °C).

Table 3
Effective activation energy ($E_{A,e}$) and pre-exponential factor (k_0) determined from Arrhenius analysis of the temperature-dependent reaction rate constant during variation of operation temperature at 1 bar_a, 1000 rpm, and a H12-BT feed rate of 2.0 ml min^{-1}. The parameters quantify the temperature sensitivity of hydrogen release under continuous slurry operation in the studied temperature range (210–250 °C).

$E_{A,e}$ / kJ mol^{-1}	k_0 / $l_{Hx\text{-}BT}$ kg_{Pt}^{-1} s^{-1}
118	1.02×10^{11}

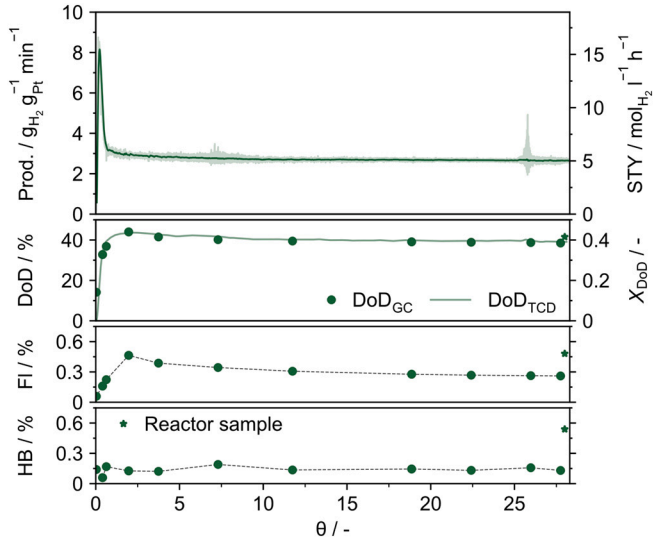

Fig. 7. Reactor performance indicators and side-product formation at elevated temperatures and pressure (310 °C, 4.3 bar_a) during operation at 1000 rpm and a H12-BT feed rate of 2.0 ml min^{-1}. The data illustrate the effect of intensified operating conditions on hydrogen productivity and accumulation of high-boiling by-products. The star indicates the reactor sample taken after cool-down. Dashed lines to guide the eye.

levels, the formation of side products is pronounced at long-term dehydrogenation when compared to the previous low-temperature experiments (Fig. S.11). Hence, the formation of high-boilers as dominating side products during the dehydrogenation of H12-BT was examined in detail (Fig. 7, Table S.11). Small amounts of methylfluorene species were detected throughout the experiment. The concentration peaked (~0.5%) in the beginning of the experiment alongside the rise of the DoD and gradually decreased to a stable concentration of ~0.3%. In comparison to impurities in the liquid feed, the share of other high-boiling compounds remained constant (~0.1%). As methylfluorene is formed through the deep dehydrogenation of H6-BT and H0-BT species, and subsequent intramolecular oxidative dehydrocyclisation,[34] the formation correlates with the concentration of these species. The subsequent decrease in methylfluorene concentration can be attributed to the reduced availability of H6-BT and H0-BT as the system approaches steady-state at slightly lower DoD. In addition, consecutive reactions such as further condensation or polymerisation of methylfluorene to heavier polyaromatic hydrocarbons, as well as potential adsorption on the catalyst surface, may contribute to a reduced detectable concentration in the liquid outlet. The reactor sample, i.e. a fraction of the liquid remaining in the reactor after shutdown of the experiment, contained a significant increased concentration of heavy-boiling components (+292%) and methylfluorene (+85%) when compared to the liquid samples at the system outlet. These findings indicate that methylfluorene and other side products accumulated in the reactor, likely due to the lower vapour pressure and higher boiling points compared to H12-BT and partially dehydrogenated species. This suggests that the reactor represents a mild separation stage in which lighter and more volatile LOHC species are preferentially discharged, while strongly dehydrogenated and condensed species are retained. Noteworthy, a similar trend was observed for the DoD, which was higher in the reactor sample than at the system outlet. Since the boiling point of H0-BT is higher than the boiling point of H12-BT,[34,42,43] preferential discharge of the latter through the gas phase may be expected resulting in slightly increased DoD within the reactor, which may further promote the accumulation of highly dehydrogenated and condensed aromatic species.

When key performance indicators are compared across reactor concepts for dehydrogenation of perhydro benzyltoluene, different objectives for reactor development must be considered. Further, direct comparison under identical operation conditions is limited due to inherent differences in reactor design and reported experimental parameters. Therefore, normalised performance indicators were used. Under comparable temperature and pressure ranges of 290–330 °C and 2–5 bar, respectively, the reported Pt-based productivity typically ranges between 0.12 and 0.80 g_{H2} g_{Pt}^{-1} min^{-1}, which is substantially lower than in the present three-phase slurry reactor (Table 4). This indicates a high utilisation of the precious metal catalyst under continuous operation. In plug flow systems, only a fraction of the liquid phase is in direct contact with catalytically active surfaces due to the release of gaseous hydrogen, whereas the slurry reactor maximises liquid-catalyst contact. In contrast, fixed-bed and coated reactors achieve considerably higher space-time yields of up to ~40 mol_{H2} l^{-1} h^{-1}, reflecting incorporation of high amounts of catalyst and volumetric intensification,

Table 4
Comparison of key performance indicators for reactor concepts for perhydro benzyltoluene dehydrogenation reported in the literature, including operating conditions, catalyst inventory, Pt-based hydrogen productivity (Prod.), space-time yield (STY), and degree of dehydrogenation (DoD). STY values are based on the reported reaction volume. Direct comparison across reactor concepts should be interpreted cautiously due to differences in reactor geometry, catalyst packing density, and non-reactive volume.

Reactor type	T / °C	p / bar_a	Catalyst	m_{Pt} / g	V_R / ml	Prod. / g_{H2} g_{Pt}^{-1} min^{-1}	STY / mol_{H2} l^{-1} h^{-1}	DoD / %	Ref.
Continuous three-phase stirred tank slurry reactor	310	4.3	EleMax D	0.02	270	2.70	5.2	40.5	This work
Semi-batch autoclave	290	2.9	EleMax D	0.05	290[A]	0.80	(4.5)[B]	10–50	[34]
Semi-batch reactive-distillation	~262	1	EleMax D	0.05	318	0.48	(2.0)[B]	10–30	[17]
Fixed-bed reactor (classical design)	290	4	EleMax D	1.02	470	0.35	22.6	44	[11]
	300					0.50	32.2	63	
	310	3	EleMax D	1.02	470	0.22[C]	14.3[C]	88	[9]
		4				0.18[C]	11.5[C]	71	
		5				0.16[C]	10.4[C]	64	
		3				0.58[D]	38.1[D]	44	
		4				0.61[D]	39.8[D]	46	
		5				0.56[D]	36.3[D]	42	
Fixed-bed reactor (inverted design)	290	4	EleMax D	4.20	2355	0.29	15.4	45	[11]
	300			4.20	2355	0.39	20.7	60	
Bench-scale fixed-bed reactor	~364	n/r	PtS/Al_2O_3 (0.6 wt% Pt)	18.00	3760	0.21[E]	30.4[E]	~100	[39]
Catalytic finned-tube reactor	290	2	PtS/Al_2O_3 (5 wt% Pt)	7.10	1520	0.12	16.7	46	[23]
	310	3				0.13	18.1	74	
	330	4				0.15	20.9	87	

[A] Estimated based on 270 g H0-BT using averaged densities of H0-BT and H12-BT.
[B] Estimated STY for semi-batch systems based on geometric reaction volume. Values are only indicative, as steady-state operation is not applicable.
[C] Calculated for LHSV 0.6 h^{-1} with DoD estimated from graphical data using plot digitation.
[D] Calculated for LHSV 3.2 h^{-1} with DoD estimated from graphical data using plot digitation.
[E] Reconstructed from reported volumetric hydrogen flow rates using the ideal gas law under standard conditions (0 °C, 1 atm; 22.4 l mol^{-1}) [33].

which is targeted in, e.g., mobile applications. With a space-time-yield of 5.2 mol_{H2} l^{-1} h^{-1}, the slurry reactor exhibits a lower volumetric productivity when compared to the plug-flow systems (Table 4). However, space-time-yield strongly depends on reactor geometry and the fraction of non-reactive volume. Slurry CSTRs inherently include mixing volume and gas holdup to ensure stable three-phase operation, which reduces volumetric productivity. Hence, the slurry reactor represents a complementary reactor strategy targeting high catalyst utilisation and operational robustness rather than maximum volumetric intensification.

3.5. Re-starting behaviour

To evaluate system and operational stability, a dedicated experimental plan with multiple start-up und shutdown periods with and without argon flow was conducted (Fig. 8, Table S.12). The argon flow has no significant effect on the overall performance, but increases the accuracy of the determination of the productivity significantly. When the argon flow was switched back to the reactor, a short spike in hydrogen release was recorded due to purging of the reactor. The DoD remained mainly unaffected from the argon flow.

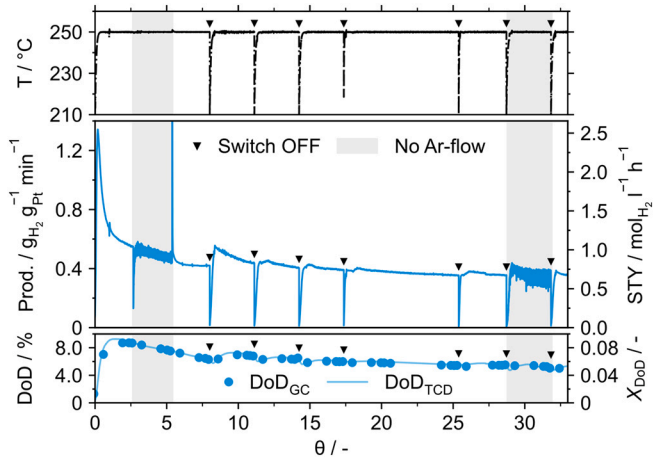

Fig. 8. Reactor performance during multiple start-up und shutdown periods at 250 °C, 1 bar_a, 1000 rpm, and a H12-BT feed rate of 2.0 ml min^{-1}. The data demonstrate the reproducibility of hydrogen productivity and stable reactor operation after repeated interruptions, highlighting the robustness of the three-phase slurry configuration under dynamic conditions.

Following the first restart, an increased productivity was observed, followed by a gradual decline and stabilisation at approx. 0.45 g_{H2} g_{Pt}^{-1} min^{-1}, which reflects the steady-state before the shutdown (0.42 g_{H2} g_{Pt}^{-1} min^{-1}). In subsequent cycles, a similar pattern was observed. The same behaviour was reflected in the DoD, which increased slightly after each restart. One possible explanation for these temporary increases is the greater availability of the hydrogenated reactant (H12-BT) during the heating process as the reactant feed is switched on during heating when reaching 210 °C.

Solymosi et al.[44] identified the nucleation of hydrogen bubbles within the pores of the catalyst as a rate-determining step in technical LOHC dehydrogenation. More interestingly, the catalytic performance of the shaped technical catalysts was strongly affected by LOHC filling the pores and supersaturation of this liquid with dissolved hydrogen, which caused an inhibited state upon intermittent cooling. The activity after restart could be recovered by a mechanical stimuli, overcoming the energy barrier required for hydrogen bubble nucleation and restoring a dynamic hydrogen release with pulsating flows of LOHC into and gaseous hydrogen out of the pores. As the full productivity was recovered after start-up in the three-phase slurry reactor, the agitation provided by the stirrer appears sufficient to sustain nucleation and recover hydrogen release. However, process stability decreased when compared to long-term operation and several cycles do not meet the steady-state criterion. Nevertheless, full recovery of hydrogen productivity was achieved in all cases following a short adaptation phase. These observations indicate that the slurry CSTR allows for reproducible restart and continued operation under dynamic conditions, although transient deviations from steady-state must be considered during cycling. Overall, the results suggest that the reactor configuration is suitable for applications involving intermittent operation, provided that stabilisation periods are accounted for in process design.

3.6. Hydrogenation

In addition to dehydrogenation, hydrogenation experiments were performed to evaluate the operability of the reactor configuration under technically relevant conditions. For stationary LOHC-based energy storage systems, practical implementation is facilitated when both hydrogen release and hydrogen uptake can be realized within the same process infrastructure.[45] The suitability of the three-phase slurry reactor for continuous hydrogenation of H0-BT was assessed in an additional experiment at 250 °C and 32.1 bar_a using a flow of 1000 ml min^{-1} of hydrogen (Fig. 9, Table S.13). Complete conversion of hydrogen was observed at the initial reactant feed rate of 2.0 ml min^{-1} for six mean residence times yielding a DoH of 63.5%, which is markedly lower than the equilibrium conversion at applied conditions (Fig. S.9, Table S.7), i.e. the provided supply of hydrogen was the actual limiting factor and the operation pressure remained below the setpoint.

The reactant feed rate was reduced stepwise to 1.0 ml min^{-1} and 0.5 ml min^{-1}. After the first decrease, unreacted H0-BT and H6-BT in the reactor was first fully hydrogenated before the operation pressure increased and stabilised at the setpoint of 32.1 bar_a. Afterwards, unconverted hydrogen was detected at the reactor outlet. Hydrogenation of the LOHC was almost complete with a DoH of 99.6% at a productivity of 0.29 $g_{H2}\ g_{Pt,Pd}^{-1}\ min^{-1}$, which corresponds to a hydrogen consumption rate of 793 ml min^{-1}. For comparison, Rüde et al.[34] reported a mean productivity of 4.6 $g_{H2}\ g_{Pt}^{-1}\ min^{-1}$ in the DoH range of 50–90% for semi-batch hydrogenation of technical H0-BT at 290 °C and 30 bar using sulfur-modified EleMax D Pt/Al_2O_3 catalyst, whereas Jorschick et al.[42] achieved up to 6.68 $g_{H2}g_{Pt}^{-1}\ min^{-1}$ for batch hydrogenation of H0-BT at 240 °C and 30 bar over a 5 wt% Pt/Al_2O_3 powder catalyst for a DoH range of 20–50%. However, direct comparison of (semi-)batch productivity with the herein reported continuous, almost complete hydrogenation is not feasible. Decreasing the reactant feed rate further to 0.5 ml min^{-1} only induced a marginal increase in DoH (99.9%), which is higher than the DoH of the technically available H12-BT used in the dehydrogenation experiments. No side products other than H6-BT were detected throughout the experiment with the final share of H6-BT being 0.1% alongside equal amounts of unconverted H0-BT. Overall, the hydrogenation experiments demonstrate stable operation of the reactor during hydrogenation and confirm the general suitability of the reactor configuration for bi-directional application, i.e. alternating hydrogen loading and unloading, which may require the use of a catalyst suitable for both directions.

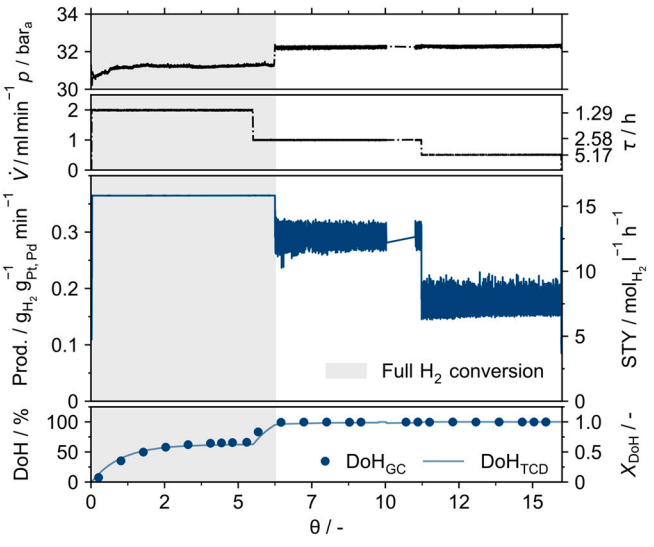

Fig. 9. Reactor performance during hydrogenation of H0-BT at 250 °C and 32.1 bar_a using a catalyst basket configuration at 1000 rpm. Key performance indicators are shown for varying H0-BT feed rates. The data demonstrate stable operation of the CSTR under hydrogen uptake conditions and illustrate the influence of residence time on hydrogenation performance.

4. Summary and conclusions

The continuous three-phase stirred tank slurry reactor investigated in this study provides a technically relevant alternative for LOHC dehydrogenation reactors with particular advantages in catalyst utilisation and operational stability during continuous operation. Compared to reported continuous reactor concepts, the system enables high Pt-based hydrogen productivity (2.7 $g_{H2}\ g_{Pt}^{-1}\ min^{-1}$) at stable conversion levels under steady-state operation. Structured benchmarking against representative fixed-bed and finned-tube reactors demonstrates that, while volumetric space-time yield is lower due to inherent mixing volume and gas holdup, precious-metal utilisation is comparatively high, reflecting a different optimisation strategy. In addition, continuous hydrogenation (DoH = 99.9%) was successfully demonstrated using a catalyst basket configuration, confirming the general suitability of the CSTR architecture for reversible LOHC operation.

A key advantage of the slurry configuration lies in the homogeneous suspension of catalyst particles, which maximises catalyst-LOHC contact and effective gas removal during hydrogen release. The reactor maintained stable productivity during long-term operation and recovered performance after restart cycles, although short stabilisation phases were observed under repeated dynamic switching. These results indicate that the three-phase CSTR supports stable operation under both steady and intermittent conditions, which is highly relevant for practical LOHC applications. The study further highlights the importance of precise control of operating parameters. Temperature, pressure, feed rate, and mixing intensity must be carefully balanced to optimise hydrogen productivity and degree of dehydrogenation while limiting side-product formation.

While the present work demonstrates stable performance at laboratory scale (~450 ml), mechanically agitated three-phase slurry CSTRs represent an established reactor class in industrial chemical manufacturing. Slurry CSTRs are commercially available across a wide size range from laboratory scale to multi-cubic-meter units, while scale-up is well-documented based on geometric similarity, solids suspension criteria, and maintenance of constant specific power input (P/V).[45–47] At larger scale, enabling efficient heat supply and homogeneous temperature control will be essential for the strongly endothermic dehydrogenation and can be implemented using established heated-vessel concepts. In addition, cascade configurations of stirred tanks provide a pathway to higher overall degrees of dehydrogenation, while maintaining moderate per-stage conversion.

As LOHC technology advances toward higher technology readiness levels, reactor concepts must enable reliable operation under flexible load conditions while maintaining efficient thermal management. The present results position the three-phase slurry CSTR as a complementary reactor strategy within LOHC technology, prioritising catalyst efficiency, thermal homogeneity, and operational robustness over maximum volumetric intensification. Future work will focus on further optimisation of catalyst formulations for slurry operation, improved heat-exchange integration, and scale-up toward industrial implementation.

Symbols

Variable	Description	Unit
$c_{H12\text{-}BT}$	Concentration of H12-BT	mol l^{-1}
$c_{Hx\text{-}BT}$	Concentration of hydrogenated BT equivalents	mol l^{-1}
c_i	Concentration of component i	mol l^{-1}
D	Impeller diameter	mm
ΔProd.	Relative change in productivity	%

(*continued on next page*)

(*continued*)

Variable	Description	Unit
Δt	Time interval	min
DoD	Degree of dehydrogenation	%
DoD_{GC}	Degree of dehydrogenation according to GC-FID	%
DoD_{TCD}	Degree of dehydrogenation according to TCD	%
DoH	Degree of hydrogenation	%
DoH_{GC}	Degree of hydrogenation according to GC-FID	%
DoH_{TCD}	Degree of hydrogenation according to TCD	%
d_p	Mass-mean particle diameter	µm
$E_{A,e}$	Arrhenius activation energy	kJ mol^{-1}
η	Dynamic Viscosity	mPas s
g	Gravitational acceleration constant	m s^{-2}
k_0	Pre-exponential factor	$l_{Hx\text{-}BT}$ kg_{Pt}^{-1} s^{-1}
k_{eff}	Effective reaction rate constant	$l_{Hx\text{-}BT}$ kg_{Pt}^{-1} s^{-1}
$m_{act.comp.}$	Mass of active catalytic component	kg
$M_{BT\text{-}mix}$	Molar mass of BT-mixture	g mol^{-1}
m_{cat}	Catalyst mass	g
m_{H2}	Mass of released hydrogen	g
M_{H2}	Molar mass of hydrogen	g mol^{-1}
m_{Pt}	Mass of platinum	g
n	Impeller rotation speed	rpm
$\dot{n}$	Molar flow of formed product	mol h^{-1}
n_{eff}	Effective reaction order	–
$n_{H0\text{-}BT}$	Moles H0-BT	mol
$n_{H0\text{-}BT,0}$	Moles H0-BT in the feed	mol
$n_{H2,\ consumed}$	Reacted moles of hydrogen	mol
$n_{H2,in}$	Molar hydrogen inflow	mol
$n_{H2,out}$	Molar hydrogen outflow	mol
$n_{H2,released}$	Released moles of hydrogen	mol
$n_{H2,rev.in}$	Moles of hydrogen reversibly bound in the LOHC inflow	mol
$n_{H2,rev.max}$	Maximum molar capacity for reversibly bound hydrogen	mol
$n_{H2,rev.out}$	Residual reversibly bound hydrogen in the LOHC outflow	mol
n_i	Molar amount of component i	mol
$n_{i,0}$	Moles of component i in the feed	mol
n_{js}	Just-suspended impeller speed	rpm
ν	Kinematic viscosity	m^2 s^{-1}
Prod.	Precious metal based productivity	g_{H2} g_{Pt}^{-1} min^{-1}
R	Universal gas constant	J mol^{-1} K^{-1}
Re	Reynolds number	–
$r_{H2,eff}$	Effective formation rate of hydrogen	mol_{H2} kg_{Pt}^{-1} s^{-1}
$r_{i,eff}$	Effective reaction rate for component i	mol $kg_{act.comp.}^{-1}$ s^{-1}
ρ	Density	kg m^{-3}
$\rho_{BT\text{-}mix}$	Density of BT-mixture	kg m^{-3}
ρ_{H2}	Density of hydrogen	kg m^{-3}
ρ_l	Density of liquid phase	kg m^{-3}
ρ_s	Density of solid phase	kg m^{-3}
S	Dimensionless number (function of impeller type)	–
STY	Space-time yield	mol_{H2} l^{-1} h^{-1}
t	Time	min
T	Temperature	K
τ	Mean residence time	h
θ	Dimensionless time	h
V	Volume	ml
V	Volumetric reactant feed rate	ml min^{-1}
V_{Ar}	Volumetric argon flow rate	ml min^{-1}
V_{H2}	Volumetric hydrogen flow rate	ml min^{-1}
V_m	Molar gas volume under standard conditions	l mol^{-1}
V_R	Reaction Volume	ml
w	Catalyst loading	wt%
x	Mass ratio of suspended solids to liquid	–
X	Conversion	–
X_{DoD}	conversion of dehydrogenation	–
X_{DoH}	conversion of hydrogenation	–
x_{Fl}	Mole fraction of methylfluorene	–
$x_{H0\text{-}BT}$	Mole fraction of H0-BT	–
$x_{H12\text{-}BT}$	Mole fraction of H12-BT	–
x_{H2}	Hydrogen volume fraction in argon	–
$x_{H6\text{-}BT}$	Mole fraction of H6-BT	–
x_{HB}	Mole fraction of other high-boiling compounds	–
x_i	Mole fraction of component i	–

CRediT authorship contribution statement

Elisabeth Herzinger: Writing – review & editing, Writing – original draft, Visualization, Validation, Methodology, Investigation, Formal analysis, Data curation, Conceptualization. **Jona Berger:** Methodology, Investigation, Formal analysis. **Moritz Wolf:** Writing – review & editing, Validation, Supervision, Resources, Project administration, Methodology, Funding acquisition, Conceptualization.

Declaration of competing interest

The authors declare that they have no known competing financial interests or personal relationships that could have appeared to influence the work reported in this paper.

Acknowledgments

Financial support by the Helmholtz Research Program “Materials and Technologies for the Energy Transition (MTET), Topic 3: Chemical Energy Carriers” and the Strategy Funds of the KIT Executive Board are highly acknowledged. Clariant and Hydrogenious LOHC Technologies are thanked for providing the commercial catalysts EleMax D and EleMax H, while Hydrogenious LOHC Technologies is also acknowledged for the provision of perhydro benzyltoluene. Appreciation is extended to Dr. Timo Schaerfe (né Rüde) for his insights into liquid sample analysis and for providing the code used to evaluate the data. Input on data management for the three-phase slurry reactor and the evaluation of kinetic parameters by Jakob Biesinger is highly acknowledged. Dr. Thomas Zevaco is thanked for the high-quality, publication-ready photographs. The mechanical workshop is gratefully acknowledged for its support in manufacturing custom components and implementing modifications to the reactor setup. Armin Lautenbach determined the metal content by inductively coupled plasma atomic emission spectrometry. Jakob Heisel provided support with CAD drawing and Christin Büsching prepared the reactor flow-scheme.

Appendix A. Supplementary data

Supplementary data to this article can be found online at https://doi.org/10.1016/j.cej.2026.175168.

Data availability

All data is openly available on Repo4Cat (https://repository.nfdi4cat.org/) via the link: https://hdl.handle.net/21.11165/4cat/97sc-ppya.

References

[1] The Intergovernmental Panel on Climate Change, AR6 Synthesis Report: Climate Change 2023, 2023.
[2] World Meteorological Organization, State of the Global Climate 2024, 2025.
[3] M.A. Sattar, M.G. Rasul, M.I. Jahirul, M.M. Hasan, An up-to-date review on the progress and challenges of hydrogen storage, and its safety and economic analysis, Sustain. Energy Fuels 8 (2024) 3545–3573, https://doi.org/10.1039/D4SE00281D.
[4] F. Li, D. Liu, K. Sun, S. Yang, F. Peng, K. Zhang, G. Guo, Y. Si, Towards a future hydrogen supply chain: a review of technologies and challenges, Sustainability 16 (2024) 1890, https://doi.org/10.3390/su1605189.
[5] A. Bárkányi, B.L. Tarcsay, L. Lovas, T. Mérő, T. Chován, A. Egedy, Future of hydrogen economy: simulation-based comparison of LOHC systems, Clean Techn. Environ. Policy 26 (2024) 1521, https://doi.org/10.1007/s10098-023-02528-w.
[6] P.C. Rao, M. Yoon, Potential liquid-organic hydrogen carrier (LOHC) systems: a review on recent progress, Energies 13 (2020) 6040, https://doi.org/10.3390/en13226040.
[7] P. Preuster, C. Papp, P. Wasserscheid, Liquid organic hydrogen carriers (LOHCs): toward a hydrogen-free hydrogen economy, Acc. Chem. Res. 50 (1) (2017) 74–85, https://doi.org/10.1021/acs.accounts.6b00474.
[8] E. Herzinger, M. Wolf, Perspectives and potential of liquid organic hydrogen carriers in the German energy scenario, Chem. Ing. Tech. 96 (2024) 65–73, https://doi.org/10.1002/cite.202300227.

[9] M. Willer, P. Preuster, M. Geißelbrecht, P. Wasserscheid, Continuous dehydrogenation of perhydro benzyltoluene and perhydro dibenzyltoluene in a packed bed vertical tubular reactor – the role of LOHC evaporation, Int. J. Hydrog. Energy 57 (2024) 1513–1523, https://doi.org/10.1016/j.ijhydene.2024.01.031.
[10] J. Geiling, M. Steinberger, F. Ortner, R. Seyfried, A. Nuß, F. Uhrig, C. Lange, R. Öchsner, P. Wasserscheid, M. März, P. Preuster, Combined dynamic operation of PEM fuel cell and continuous dehydrogenation of perhydro-dibenzyltoluene, Int. J. Hydrog. Energy 46 (2021) 35662–35677, https://doi.org/10.1016/j.ijhydene.2021.08.034.
[11] J. Kadar, F. Gackstatter, F. Ortner, L. Wagner, M. Willer, P. Preuster, P. Wasserscheid, M. Geißelbrecht, Boosting power density of hydrogen release from LOHC systems by an inverted fixed-bed reactor design, Int. J. Hydrog. Energy 59 (2024) 1376–1387, https://doi.org/10.1016/j.ijhydene.2024.02.096.
[12] A. Fikrt, R. Brehmer, V.-O. Milella, K. Müller, A. Bösmann, P. Preuster, N. Alt, E. Schlücker, P. Wasserscheid, W. Arlt, Dynamic power supply by hydrogen bound to a liquid organic hydrogen carrier, Appl. Energy 194 (2017) 1–8, https://doi.org/10.1016/j.apenergy.2017.02.070.
[13] Y. Kwak, J. Kirk, S. Moon, T. Ohm, Y.-J. Lee, M. Jang, L.-H. Park, C. Ahn, H. Jeong, H. Sohn, S.W. Nam, C.W. Yoon, Y.S. Jo, Y. Kim, Hydrogen production from homocyclic liquid organic hydrogen carriers (LOHCs): benchmarking studies and energy-economic analyses, Energy Convers. Manag. 239 (2021) 114124, https://doi.org/10.1016/j.enconman.2021.114124.
[14] A. Wunsch, T. Berg, P. Pfeifer, Hydrogen production from the LOHC Perhydro-Dibenzyl-toluene and purification using a 5 µm PdAg-membrane in a coupled microstructured system, Materials 13 (2020) 277, https://doi.org/10.3390/ma13020277.
[15] A. Wunsch, M. Mohr, P. Pfeifer, Intensified LOHC-dehydrogenation using multi-stage microstructures and Pd-based membranes, Membranes (Basel) 8 (2018) 112, https://doi.org/10.3390/membranes8040112.
[16] A. Wunsch, P. Kant, M. Mohr, K. Haas-Santo, P. Pfeifer, R. Dittmeyer, Recent developments in compact membrane reactors with hydrogen separation, Membranes (Basel) 8 (2018) 107, https://doi.org/10.3390/membranes8040107.
[17] M. Geißelbrecht, S. Mrusek, K. Müller, P. Preuster, A. Bösmann, P. Wasserscheid, Highly efficient, low-temperature hydrogen release from perhydro-benzyltoluene using reactive distillation, Energy Environ. Sci. 13 (2020) 3119–3128, https://doi.org/10.1039/D0EE01155J.
[18] T. Rüde, Y. Lu, L. Anschütz, M. Blasius, M. Wolf, P. Preuster, P. Wasserscheid, M. Geißelbrecht, Performance of continuous hydrogen production from Perhydro Benzyltoluene by catalytic distillation and heat integration concepts with a fuel cell, Energ. Technol. 11 (2023) 2201366, https://doi.org/10.1002/ente.202201366.
[19] L. van Hoecke, N.B. Kummamuru, H. Pourfallah, S.W. Verbruggen, P. Perreault, Intensified swirling reactor for the dehydrogenation of LOHC, Int. J. Hydrog. Energy 51 (2024) 611–623, https://doi.org/10.1016/j.ijhydene.2023.08.150.
[20] J. Lee, M. Usman, S. Park, S. Lee, M.H. Song, Development of dehydrogenation system for liquid organic hydrogen carrier with enhanced reaction rate, Appl. Sci. 14 (2024) 5803, https://doi.org/10.3390/app14135803.
[21] T. Solymosi, F. Auer, S. Dürr, P. Preuster, P. Wasserscheid, Catalytically activated stainless steel plates for the dehydrogenation of perhydro dibenzyltoluene, Int. J. Hydrog. Energy 46 (2021) 34797–34806, https://doi.org/10.1016/j.ijhydene.2021.08.040.
[22] W. Peters, M. Eypasch, T. Frank, J. Schwerdtfeger, C. Körner, A. Bösmann, P. Wasserscheid, Efficient hydrogen release from perhydro-N-ethylcarbazole using catalyst-coated metallic structures produced by selective electron beam melting, Energy Environ. Sci. 8 (2015) 641–649, https://doi.org/10.1039/C4EE03461A.
[23] A. Ellert, M. Schmacks, M.J. Braun, L. Piccirilli, T.V.W. Janssens, P. Wasserscheid, P. Schühle, Continuous dehydrogenation of Perhydro Benzyltoluene in a catalytic finned tube reactor, Ind. Eng. Chem. Res. 64 (2025) 3714–3727, https://doi.org/10.1021/acs.iecr.4c04254.
[24] C. Prieto, A. Sánchez, M. Martín, A three-phase reactor assessment for the deployment of liquid organic hydrogen carriers (LOHCs): dybenzyltoluene and indoles mixture systems as case studies, Energy Convers. Manag. 294 (2023) 117548, https://doi.org/10.1016/j.enconman.2023.117548.
[25] O. Levenspiel, Chemical Reaction Engineering, third ed., John Wiley & Sons, New York, 1999.
[26] M.A. Köhler, Comparison of mechanically agitated and bubble column slurry reactors, Appl. Catal. 22 (1) (1986) 21–53, https://doi.org/10.1016/S0166-9834(00)82593-2.
[27] J.M. Coulson, J.F. Richardson, Chemical Engineering, sixth ed., Elsevier Butterworth-Heinemann, Oxford, 1983.
[28] E.L. Paul, V.A. Atiemo-Obeng, S.M. Kresta, Handbook of Industrial Mixing: Science and Practice, Wiley-Interscience, Hoboken N.J., 2004.
[29] D.B. Newell, E. Tiesinga, The International System of Units (SI), National Institute of Standards and Technology, Gaithersburg, MD, 2019.
[30] C. Devarajulu, M. Loganathan, Effect of impeller clearance and liquid level on critical impeller speed in an agitated vessel using different axial and radial impellers, J. Appl. Fluid Mech. 9 (2016) 2753–2761, https://doi.org/10.29252/jafm.09.06.24824.
[31] Ullmann's Encyclopedia of Industrial Chemistry, Wiley, 2003.
[32] G. Emig, E. Klemm, H. Freund, Chemische Reaktionstechnik, Springer Berlin Heidelberg, Berlin, Heidelberg, 2024.
[33] P.J. Mohr, B.N. Taylor, CODATA recommended values of the fundamental physical constants: 1998, Rev. Mod. Phys. 72 (2) (2000) 351–495, https://doi.org/10.1103/RevModPhys.72.351.
[34] T. Rüde, S. Dürr, P. Preuster, M. Wolf, P. Wasserscheid, Benzyltoluene/perhydro benzyltoluene – pushing the performance limits of pure hydrocarbon liquid organic hydrogen carrier (LOHC) systems, sustain, Energy Fuel 6 (2022) 1541–1553, https://doi.org/10.1039/D1SE01767E.
[35] R. Garidzirai, P. Modisha, D. Bessarabov, Assessment of reaction kinetics for the dehydrogenation of Perhydro-Dibenzyltoluene using Mg- and Zn-modified Pt/Al_2O_3 catalysts, Catalysts 14 (2024) 32, https://doi.org/10.3390/catal14010032.
[36] R. Peters, R. Deja, Q. Fang, N. van Nguyen, P. Preuster, L. Blum, P. Wasserscheid, D. Stolten, A solid oxide fuel cell operating on liquid organic hydrogen carrier-based hydrogen – a kinetic model of the hydrogen release unit and system performance, Int. J. Hydrog. Energy 44 (2019) 13794–13806, https://doi.org/10.1016/j.ijhydene.2019.03.220.
[37] H. Jorschick, S. Dürr, P. Preuster, A. Bösmann, P. Wasserscheid, Operational stability of a LOHC-based hot pressure swing reactor for hydrogen storage, Energy Tech. 7 (2019) 146–152, https://doi.org/10.1002/ente.201800499.
[38] P. Modisha, P. Gqogqa, R. Garidzirai, C.N. Ouma, D. Bessarabov, Evaluation of catalyst activity for release of hydrogen from liquid organic hydrogen carriers, Int. J. Hydrog. Energy 44 (2019) 21926–21935, https://doi.org/10.1016/j.ijhydene.2019.06.212.
[39] I.S. Lim, Y. Jeong, Y. Kwak, E.-R. On, Q.N. Dao, H. Jeong, H. Sohn, S.W. Nam, T.-H. Lim, K. Müller, Y. Kim, Maximizing clean hydrogen release from perhydro-benzyltoluene: energy-efficient scale-up strategies and techno-economic analyses, Chem. Eng. J. 478 (2023) 147296, https://doi.org/10.1016/j.cej.2023.147296.
[40] K.C. Musavuli, P. Modisha, R.C. Everson, A. Malakhov, D. Bessarabov, Metal foam as surface-extended catalyst support structure for process intensification in the dehydrogenation of Perhydro-Dibenzyltoluene on a Pt/Al_2O_3 catalyst, Catalysts 15 (2025) 44, https://doi.org/10.3390/catal15010044.
[41] S. Park, M. Naseem, S. Lee, Experimental assessment of Perhydro-Dibenzyltoluene dehydrogenation reaction kinetics in a continuous flow system for stable hydrogen supply, Materials (Basel) 14 (2021), https://doi.org/10.3390/ma14247613.
[42] H. Jorschick, M. Geißelbrecht, M. Eßl, P. Preuster, A. Bösmann, P. Wasserscheid, Benzyltoluene/dibenzyltoluene-based mixtures as suitable liquid organic hydrogen carrier systems for low temperature applications, Int. J. Hydrog. Energy 45 (2020) 14897–14906, https://doi.org/10.1016/j.ijhydene.2020.03.210.
[43] T.W. Kim, Y. Jo, K. Jeong, H. Yook, J.W. Han, J.H. Jang, G.B. Han, J.H. Park, Y.-W. Suh, Tuning the isomer composition is a key to overcome the performance limits of commercial benzyltoluene as liquid organic hydrogen carrier, J. Energy Storage 60 (2023) 106676, https://doi.org/10.1016/j.est.2023.106676.
[44] T. Solymosi, M. Geißelbrecht, S. Mayer, M. Auer, P. Leicht, M. Terlinden, P. Malgaretti, A. Bösmann, P. Preuster, J. Harting, M. Thommes, N. Vogel, P. Wasserscheid, Nucleation as a rate-determining step in catalytic gas generation reactions from liquid phase systems, Sci. Adv. 8 (2022), https://doi.org/10.1126/sciadv.ade3262.
[45] N. Cherkasov, S.J. Adams, E.G.A. Bainbridge, J.A.M. Thornton, Continuous stirred tank reactors in fine chemical synthesis for efficient mixing, solids-handling, and rapid scale-up, React. Chem. Eng. 8 (2023) 266–277, https://doi.org/10.1039/D2RE00232A.
[46] M. Kraume, P. Zehner, Concept for scale-up of solids suspension in stirred tanks, Can. J. Chem. Eng. 80 (2002) 1–8, https://doi.org/10.1002/cjce.5450800413.
[47] S. Harrison, A. Kotsiopoulos, R. Stevenson, J.J. Cilliers, Mixing indices allow scale-up of stirred tank slurry reactor conditions for equivalent homogeneity, Chem. Eng. Res. Des. 153 (2020) 865–874, https://doi.org/10.1016/j.cherd.2019.10.049.